PERGAMON

International Journal of Heat and Mass Transfer 43 (2000) 1373–1389

International Journal of HEAT and MASS TRANSFER

www.elsevier.com/locate/ijhmt

A finite element free convection model for the side wall heated cavity

K.A.R. Ismail [a,*], V.L. Scalon [b]

[a] UNICAMP-FEM-DETF, Caixa Postal 6122, Campinas, Brazil
[b] UNESP-FE-DEM, Av. Luiz EC Coube, s/n, Bauru (SP), Brazil

Received 8 October 1998; received in revised form 28 June 1999

Abstract

This paper presents a finite element numerical solution of free convection in a cavity with side walls maintained at constant but different temperatures. The predictions from the model and the method of solution were validated by comparison with the 'bench mark'solution and Vahl Davis' results and good agreement was found. The present model was used to obtain additional results over a wide range of Rayleigh number (10^3–10^6) and L/H ratios varying from 0.1 to 1.0. The predicted stream function patterns, temperature and velocity profiles as well as the mean Nusselt number were presented and discussed.

1. Introduction

The continuous increase of the processing speed and the storage capacity of the new computers, also led to the increase of the possible solutions of complex problems which involve flow with heat and mass convection as well as boundary deformation. Traditionally a great deal of complicated combined thermal fluid flow problems are solved by the control volume method based upon the finite differences approximation, even when there is no urge for fast processing machine. The use of the co-localized or equal order methods changed this situation and, more frequent, methods based upon finite element methods are preferred by research workers in the heat and fluid flow area.

One of the pioneer studies in this area is the work due to Marshall, Heinrich and Zienkiewicz [1] in which a formulation based upon a 'penalty function' was used to obtain a solution for a convective problem in a square cavity and presented results for different Rayleigh numbers (10^4, 10^5, 10^6 and 10^7).

Different possible solutions suitable for handling fluid movement by using co-localized grids were compiled and presented by Schneider et al. [2]. They examined and incorporated into their solution of several test problems using the penalty function method, the false compressibility method and the velocity correction procedure. They concluded that the method of correcting the velocity rendered the best results. Although there is a possibility of direct solution of the velocity, temperature and pressure fields for this kind of problems, it's rarely used. The most common methods can be found in Gresho [3] and Gresho and Chan [4].

Abbreviations: CVFEM, control volume finite element method.

* Corresponding author. Fax: +55-19-239-3722.
E-mail addresses: kamal@fem.unicamp.br (K.A.R. Ismail), scalon@bauru.unesp.br (V.L. Scalon).

0017-9310/00/$ - see front matter
PII: S0017-9310(99)00225-2

Nomenclature

c	specific heat (J/kg K)
$[C]$	matrix of the convective terms
k	thermal conductivity (W/m K)
K_p	term associated with pressure in the momentum equation
$[K]$	conductance matrix
L	characteristic length of the problem
$[M]$	global mass matrix
N_i	interpolation function
Nu	Nusselt number ($Nu=(hL/k)$)
p	pressure (Pa)
P	dimensionless pressure ($P=(p/\rho)(L/\alpha)^2$)
$[P_z']$	matrix of the pressure terms in z direction
Pr	Prandtl number ($Pr=(\nu/\alpha)$)
Ra	Rayleigh number ($Ra=(g\beta\Delta TL^3/\nu^2)Pr$)
$s^{p,z}$	the source term associate to the pressure in z direction
S	source term
t	time (s)
T	temperature (°C)
u	velocity in the x direction (m/s)
U	dimensionless velocity in the x direction ($U=(uL/\alpha)$)
v	velocity in the y direction (m/s)
V	dimensionless velocity in the y direction ($V=(vL/\alpha)$)
W	arbitrary weighting function
x	x-coordinate (m)
X	dimensionless x-coordinate ($X=(x/L)$)

Greek symbols

α	thermal diffusivity (m^2/s)
β	coefficient of thermal expansion (K^{-1})
Γ	surface of the problem
ϵ	residual value
ρ	density (kg/m^3)
τ	dimensionless time ($\tau=Fo=\alpha t/L^2$)
θ	dimensionless temperature ($\theta=(T-T_f)/(T_h-T_f)$)
Ω	problem domain
Ω_e	elementary domain
μ	dynamic viscosity (kg/m s)
ν	kinematic viscosity (m^2/s)
ψ	streamline function

Subscripts

max	maximum value
med	mean value

Studies realized by Prakash [5] and Perıc et al. [6], show that methods of equal order are more accurate. Among the most know methods with co-localized grids is the method proposed by Rice and Schnipke [7], which utilizes a transposition of the traditional control volume methods to the finite element technique. Another well known method is the time explicit method proposed by Kovacs and Kawahara [8], which was adapted for use with second order Runge Kutta by Ren and Utnes [9]. The third solution method equally important is the method proposed by Despotis and Tsangaris [10]. These solution methods can be adapted to use with upwind approximation technique, such as proposed by Brooks and Hughes [11] or the method due to Rice and Shnipke [12]. Following similar trends of the solution methods, there are a variety of alternative techniques based upon the control volume applied to finite elements method (CVFEM) originated from the studies due to Baliga and Patankar [13,14]. This method was originally proposed to use with different interpolation orders but later was adapted to incorporate co-localized grids, as done by Prakash and Patankar [15]. A complete analysis of the alternative solutions by this method can be found in Saabas and Baliga [16], while the study presented by Idelsohn and Oñate [17] addresses the question of the choice of the more suitable method to solve a specific proposed problem.

Vahl Davis and Jones [18], presented the results of innumerous methods of solution applied to a test problem of free convection in a cavity for different Rayleigh number. Later Vahl Davis [19] presented a solution for the proposed free convection problem. He obtained results for different grids extrapolated in such a way to obtain a solution with minimum possible error and, hence this solution is considered as a reference solution for this specific problem.

This paper presents a solution of free convection problem based on extending the finite element model proposed by Rice and Schnipke [7] (no free convection was admitted). The extension of their model was realized by including the necessary terms for the treatment of free convection flows and their correct manipulation. As an advantage of the present method is the use of primitive variables which facilitates the application of the boundary conditions and also the utilization of the false transient scheme which permits better convergence levels. The results are analyzed and compared with Vahl Davis' model [19] bench mark solution to validate the present method of solution.

2. Formulation of the problem

With the reference to Fig. 1, one can write the two-dimensional Navier–Stokes equations for the incompressible fluid with the energy equation in the form:

$$\left.\begin{aligned}
\rho\frac{\partial u}{\partial t}+\rho u\frac{\partial u}{\partial x}+\rho v\frac{\partial u}{\partial y}&=-\frac{\partial p}{\partial x}+\mu\left(\frac{\partial^2 u}{\partial x^2}+\frac{\partial^2 u}{\partial y^2}\right)+S_x\\
\rho\frac{\partial v}{\partial t}+\rho u\frac{\partial v}{\partial x}+\rho v\frac{\partial v}{\partial y}&=-\frac{\partial p}{\partial y}+\mu\left(\frac{\partial^2 v}{\partial x^2}+\frac{\partial^2 v}{\partial y^2}\right)+S_y\\
\rho c\frac{\partial T}{\partial t}+\rho uc\frac{\partial T}{\partial x}+\rho vc\frac{\partial T}{\partial y}&=k\left(\frac{\partial^2 T}{\partial x^2}+\frac{\partial^2 T}{\partial y^2}\right)+S_e
\end{aligned}\right\} \tag{1a}$$

where the source term of the momentum equation can include the gravitational effects. The continuity equation can be written as:

$$\frac{\partial u}{\partial x}+\frac{\partial u}{\partial y}=0 \tag{1b}$$

Notice that the momentum equations are identical to the energy equation, except for the pressure term, which can be included in the source term. In this manner applying the weighted residuals formulation to the weak form of the equation, the Galerkin discretization considering a totally implicit form, the resulting linear system can be present by:

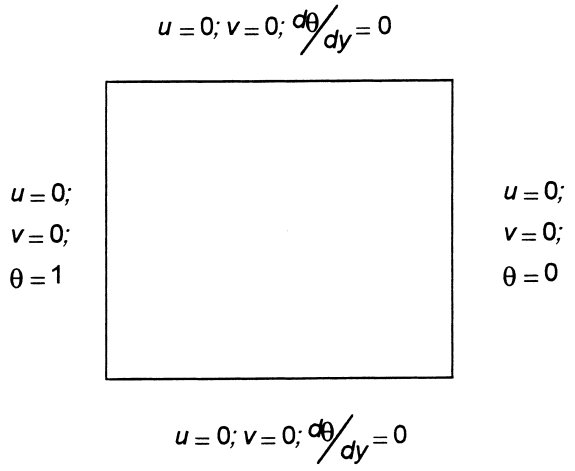

Fig. 1. Layout of the problem.

$$\{S\}=\int_\Omega N_i\times \mathrm{d}\Omega\times\vec{S} \tag{4}$$

If the indicated operations are performed on the matrices one can obtain a linear system of the form:

$$[\bar{A}_\phi]\times\{\phi\}=\{B_\phi\} \tag{5}$$

where $[\bar{A}_\phi]$ and $\{\bar{B}_\phi\}$ are identified with the respective variables: u, v or T. In this solution the temperature field is the first to be solved, since it is necessary to determine the values of the source terms in the momentum equations. This system of equations will be later used in the discretization of the continuity equation.

$$\left.\begin{aligned}
\left(\frac{1}{\Delta t}[M]+[C]+\nu[K]\right)\{u\}&=\frac{1}{\Delta t}[M]\{u^0\}+\frac{1}{\rho}\{S_x\}-\frac{1}{\rho}[M]\frac{\partial p}{\partial x}+\nu\int_\Gamma N_i\frac{\partial u}{\partial n}\mathrm{d}\Gamma\\
\left(\frac{1}{\Delta t}[M]+[C]+\nu[K]\right)\{v\}&=\frac{1}{\Delta t}[M]\{v^0\}+\frac{1}{\rho}\{S_y\}-\frac{1}{\rho}[M]\frac{\partial p}{\partial y}+\nu\int_\Gamma N_i\frac{\partial v}{\partial n}\mathrm{d}\Gamma\\
\left(\frac{1}{\Delta t}[M]+[C]+\alpha[K]\right)\{T\}&=\frac{1}{\Delta t}[M]\{T^0\}+\frac{1}{\rho c}\{S_e\}+\alpha\int_\Gamma N_i\frac{\partial T}{\partial n}\mathrm{d}\Gamma
\end{aligned}\right\} \tag{1c}$$

where the values of the matrices $[M]$, $[C]$, $[K]$ and $\{S\}$ are given by:

$$[M]=\int_\Omega N_i\times \mathrm{d}\Omega \tag{1}$$

$$[C]=\int_\Omega\left(N_k u_k N_i\frac{\partial N_j}{\partial x}+N_k v_k N_i\frac{\partial N_j}{\partial y}\right)\times \mathrm{d}\Omega \tag{2}$$

$$[K]=\int_\Omega\left(\frac{\partial N_i}{\partial x}\frac{\partial N_j}{\partial x}+\frac{\partial N_i}{\partial y}\frac{\partial N_j}{\partial y}\right)\times \mathrm{d}\Omega \tag{3}$$

In this work a better approximation of the pressure fields was adopted and the expression which appears in the general equation can be approximated by

$$\int_\Omega W\frac{\partial p}{\partial z}\times \mathrm{d}\Omega=\int_\Omega W\frac{\partial N_j}{\partial z}\times \mathrm{d}\Omega\times p_j$$
$$=\int_\Omega N_i\frac{\partial N_j}{\partial z}\times \mathrm{d}\Omega\times p_j$$

where z is an arbitrary direction. In this manner a new matrix can be defined as:

$$[P'_z] = \int_\Omega N_i \frac{\partial N_j}{\partial z} \times d\Omega \tag{6}$$

Hence, the general two dimensional expression for the momentum equation can be written as:

$$\left(\frac{1}{\Delta t}[M] + [C] + \nu[K]\right)\{u\} = \frac{1}{\Delta t}[M]\{u^0\} + \frac{1}{\rho}\{S_x\} - \frac{1}{\rho}[P'_x]\{p\} + \nu\int_\Gamma N_i \frac{\partial u}{\partial n} d\Gamma \tag{7}$$

$$\left(\frac{1}{\Delta t}[M] + [C] + \nu[K]\right)\{v\} = \frac{1}{\Delta t}[M]\{v^0\} + \frac{1}{\rho}\{S_y\} - \frac{1}{\rho}[P'_y]\{p\} + \nu\int_\Gamma N_i \frac{\partial v}{\partial n} d\Gamma \tag{8}$$

Similarly, treating the continuity equation by using the method of weighted residuals, it can be written in the form

$$\varepsilon = \int_\Omega W\left(\frac{\partial u}{\partial x} + \frac{\partial u}{\partial y}\right) \times d\Omega$$

which in its weak form becomes:

$$\int_\Omega \left(\frac{\partial W}{\partial x}u + \frac{\partial W}{\partial y}v\right) \times d\Omega = \int_\Gamma W u_n \times d\Gamma \tag{9}$$

where u_n is the velocity normal to the element face and remembering that this term is only used at the domain frontiers.

One can observe that the discretized equations establish a relation between the velocity field and the pressure gradients. If we consider Eq. (5) and the load matrices $\{B_x\}$ and $\{B_y\}$ in the form:

$$\{B_z\} = -\frac{1}{\rho}[M]\frac{\partial p}{\partial z} + s_i^{p,z} = -b_i\frac{\partial p}{\partial z} + s_i^{p,z}$$

where the first term represents the load portion due to pressure while the second part represents the contribution due to the transient and the source terms.

In the matrix form, one can write the momentum equations in the form:

$$a_{i,i}u_i = -\sum_{j\neq i} a_{i,j}u_j - b_i\frac{\partial p}{\partial x} + s_i^{p,x} \tag{10a}$$

If we define a set of new variables in the form:

$$\hat{u}_i = -\frac{\sum_{j\neq i} a_{i,j}u_j}{a_{i,i}}; \quad \hat{v}_i = -\frac{\sum_{j\neq i} a_{i,j}v_j}{a_{i,i}}; \quad K_{p,i} = \frac{b_i}{a_{i,i}}; \quad S_i^{p,z} = \frac{s_i^{p,z}}{a_{i,i}} \tag{10b}$$

one can write Eq. (10a) in the form:

$$u_i = \hat{u}_i + S_i^{p,x} - K_{p,i}\frac{\partial p}{\partial x} \tag{11}$$

$$v_i = \hat{v}_i + S_i^{p,y} - K_{p,i}\frac{\partial p}{\partial y} \tag{12}$$

Since the values of u and v can be expressed in terms of the interpolation functions N_j, as:

$$u = N_j u_j = N_j\left(\hat{u}_j + S_j^{p,x} - K_{p,j}\frac{\partial p}{\partial x}\right) \text{ and}$$

$$v = N_j v_j = N_j\left(\hat{v}_j + S_j^{p,y} - K_{p,j}\frac{\partial p}{\partial y}\right)$$

these expressions can be substituted into the weak form of the continuity equation, to obtain:

$$\int_\Omega \left[\frac{\partial N_i}{\partial x}N_j\left(\hat{u}_j + S_j^{p,x} - K_{p,j}\frac{\partial p}{\partial x}\right) + \frac{\partial N_i}{\partial y}N_j\left(\hat{v}_j + S_j^{p,y} - K_{p,j}\frac{\partial p}{\partial y}\right)\right] \times d\Omega = \int_\Gamma W u_n \times d\Gamma \tag{13a}$$

Note that the pressure term in the element can be also expressed in terms of interpolation function, as:

$$p = N_i(x,y)P_i \Longrightarrow \begin{cases} \dfrac{\partial p}{\partial x} = \dfrac{\partial N_i(x,y)}{\partial x}p_i \\ \dfrac{\partial p}{\partial y} = \dfrac{\partial N_i(x,y)}{\partial y}p_i \end{cases}$$

which when substituted into Eq. (13a) one can obtain the general expression for the continuity equation in the form:

$$\int_\Omega \left[\frac{\partial N_i}{\partial x}(N_j K_{p,j})\frac{\partial N_k}{\partial x} + \frac{\partial N_i}{\partial y}(N_j K_{p,j})\frac{\partial N_k}{\partial y}\right] \times d\Omega \times p_k = \int_\Omega \left[\frac{\partial N_i}{\partial x}N_j(\hat{u}_j + S_j^{p,x}) + \frac{\partial N_i}{\partial y}N_j(\hat{v}_j + S_j^{p,y})\right] \times d\Omega - \int_\Gamma W u_n \times d\Gamma \tag{13b}$$

Considering that the vectors P_i and the $K_{p,j}$ are constants for a given element and consequently can be put outside the integral sign, the problem is reduced to a system of equations of the form:

$$[\bar{A}_p] \times \{p\} = \{B_p\} \tag{14}$$

the terms $[\bar{A}_p]$ and $\{\bar{B}_p\}$ must be given by the relations below

$$[\bar{A}_b] = \int_\Omega \left[\frac{\partial N_i}{\partial x}\frac{\partial N_j}{\partial x} + \frac{\partial N_i}{\partial y}\frac{\partial N_j}{\partial y} \right] (N_l K_{p,l}) \times \mathrm{d}\Omega$$

$$\{B_p\} = \int_\Omega \frac{\partial N_i}{\partial x} N_j \times \mathrm{d}\Omega \times (\hat{u}_j + S_j^{p,x}) + \int_\Omega \frac{\partial N_i}{\partial y} N_j \times \mathrm{d}\Omega \times (\hat{v}_j + S_j^{p,y}) - \int_\Gamma W u_n \times \mathrm{d}\Gamma$$

When the pressure field is determined one can correct the velocity field before calculating the new coefficients, this can be done as:

$$u_j = \hat{u}_j + S_j^{p,x} - \frac{1}{\rho \times a_{i,i}} \int_\Omega W \frac{\partial p}{\partial x} \times \mathrm{d}\Omega \tag{15}$$

$$v_j = \hat{v}_j + S_j^{p,y} - \frac{1}{\rho \times a_{i,i}} \int_\Omega W \frac{\partial p}{\partial y} \times \mathrm{d}\Omega \tag{16}$$

Alternatively one can interpolate the pressure field and use the Galerkin approximation in the same way as used in the case of the momentum equation to obtain the following relations:

$$u_j = \hat{u}_j + S_j^{p,x} - \frac{1}{\rho \times a_{i,i}} [P'_x]\{p\} \tag{15a}$$

$$v_j = \hat{v}_j + S_j^{p,y} - \frac{1}{\rho \times a_{i,i}} [P'_y]\{p\} \tag{16a}$$

Having defined the system of equations to be solved, it is necessary to establish the boundary conditions of the problem. In case of the momentum equation one can use the no-slip condition or the condition of known velocity. Both can be applied simply by changing the corresponding lines in the matrix to the value of interest. The boundary conditions at exit are more difficult to establish because the velocity profile is not known and the condition most used is $(\mathrm{d}\vec{u}_\mathrm{n}/\mathrm{d}\vec{n}) = 0$, because it does not need any further correction.

In the case of the pressure equation, the boundary conditions are more difficult. It was demonstrated that to obtain the weak form of the continuity equations, the term $\int_S W u_\mathrm{n} \times \mathrm{d}S$ has to be evaluated in terms of the predetermined velocity distribution. It must be mentioned that this term represents the normal velocity and hence need to be evaluated at the frontiers where mass influx or efflux occurs.

Finally, the points of the frontier can not be calculated in the same way as the internal grid points. In this case K_p of the frontier points is considered zero. This consideration implies that the $\hat{u}$ and $\hat{v}$ values according to Eqs. (11) and (12), are equal to the values specified for u and v at the frontier.

3. Results and discussion

As mentioned earlier, the method of solution is validated by comparing predictions from the present method with the results due to Vahl Davis and Jones [18] and Vahl Davis [19]. This was realized by compiling the Vahl Davis method for the problem shown in Fig. 1. He solved this problem of natural convection using a formulation based upon a vorticity and stream function method and obtained solutions for different size grids. From these results the author obtained his solution (considered as standard) by extrapolating the grids until achieving precise results. The proposed problem is a closed cavity with the two vertical walls maintained at different temperatures, as shown in Fig. 1, while the top and bottom surfaces are thermally insulated.

The numerical predictions were obtained by using a grid of 21×21 points and the results were further interpolated by a cubic spline. The grid size was chosen in order to be able to compare with Vahl Davis' results under the same conditions. Numerical trials were performed to establish the grid size most suitable for the present study. No further attempts were realized since the 21×21 grid (the same used by Vahl Davis) gave satisfactory results. Obviously for high values of Rayleigh number the errors encountered are appreciable and hence it is necessary to perform some grid size testing in order to establish a suitable grid size.

Table 1 shows the predicted values from the present solution as compared with the bench mark solution and the solution due to Vahl Davis [19] for different values of Rayleigh numbers and a fixed grid of 21×21. The analysis of the results in Table 1 shows that the predictions from the present method indicate smaller errors as compared with Vahl Davis' results except for the case of Rayleigh number 10^3, where Vahl Davis' results are in good agreement with the bench mark solution. This is principally due to the fact that Vahl Davis' formulation is based upon the vorticity and stream function. As the Rayleigh number is increased the errors associated with the solution also increase reaching values of about 23% (Vahl Davis) as compared to 12% from the present model. These

errors can be reduced without any difficulties by using finer grid size.

It is interesting to mention that the values of ψ were obtained by the numerical integration of the velocity using the trapezoidal method. Each ψ value is calculated as an average of the values for the point under consideration, integrating u along the y-coordinate and v along the x-coordinate. The value at the mean point of the cavity was also obtained by integrating the spline functions of the velocities. These results are shown in Fig. 2 illustrating the flow patterns and the constant temperature lines.

The comparative results confirm the validity of the proposed solution and the present predictions are found to compare well with the available established data. Having established the validity of the model, a study the influence of the geometry of the cavity on the stream function, velocity and temperature fields as well as the Nusselt number. Fig. 3 shows the stream function and the temperature profiles for different geo-

Table 1
Comparative values for the cavity solution

	ψ_{avg}	ψ_{max}	U_{max}	V_{max}	Nu_{max}	Nu_{min}	Nu_{avg}
$Ra = 1 \times 10^3$							
Bench mark solution	1.174	...	3.649	3.697	1.505	0.692	1.118
(Position)		(...)	$y = 0.813$	$x = 0.178$	$y = 0.092$	$y = 1$	
Vahl Davis solution	1.174	...	3.589	3.629	1.491	0.702	1.111
Error	0.00%	...	1.64%	1.84%	0.93%	1.45%	0.63%
(Position)		(...)	$y = 0.811$	$x = 0.181$	$y = 0.112$	$y = 1$	
Obtained solution	1.159[a]	...	3.645	3.695	1.496	0.696	1.115
Error	1.28%	...	0.11%	0.05%	0.60%	0.58%	0.27%
(Position)		(...)	$y = 0.814$	$x = 0.178$	$y = 0.084$	$y = 1$	
$Ra = 1 \times 10^4$							
Bench mark solution	5.071	...	16.178	19.617	3.528	0.586	2.243
(Position)		(...)	$y = 0.823$	$x = 0.119$	$y = 0.143$	$y = 1$	
Vahl Davis solution	5.176	...	16.189	19.197	3.603	0.61	2.212
Error	2.07%	...	0.07%	2.14%	2.13%	4.10%	1.38%
(Position)		(...)	$y = 0.82$	$x = 0.125$	$y = 0.165$	$y = 1$	
Obtained solution	5.01[b]	...	16.158	19.827	3.529	0.592	2.256
Error	1.20%	...	0.12%	1.07%	0.03%	1.02%	0.58%
(Position)		(...)	$y = 0.823$	$x = 0.119$	$y = 0.15$	$y = 1$	
$Ra = 1 \times 10^5$							
Bench mark solution	9.111	9.612	34.73	68.59	7.717	0.729	4.519
(Position)		(0.285, 0.601)	$y = 0.855$	$x = 0.066$	$y = 0.081$	$y = 1$	
Vahl Davis solution	9.702	10.236	36.46	62.79	7.901	0.797	4.45 + 4
Error	6.49%	6.49%	4.98%	8.46%	$y = 0.0238$	9.33%	1.44%
(Position)		(0.29, 0.60)	$y = 0.854$	$x = 0.075$	0.133	$y = 1$	
Obtained solution	8.786[c]	9.241	33.421	70.44	7.812	0.744	4.651
Error	3.57%	3.86%	3.77%	2.70%	1.23%	2.06%	2.92%
(Position)		(0.70, 0.40)[d]	$y = 0.853$	$x = 0.0672$	$y = 0.103$	$y = 1$	
$Ra = 1 \times 10^6$							
Bench mark solution	16.32	16.75	64.63	219.36	17.925	0.989	8.8
(Position)		(0.149, 0.547)	$y = 0.85$	$x = 0.0379$	$y = 0.0378$	$y = 1$	
Vahl Davis solution	20.16	20.914	79.27	195.44	14.215	1.749	9.027
Error	23.53%	24.86%	22.65%	10.90%	20.70%	76.85%	2.58%
(Position)		(0.149, 0.554)	$y = 0.862$	$x = 0.0447$	$y = 0.124$	$y = 1$	
Obtained solution	14.29[e]	14.967	57.22	220.48	15.601	0.971	8.934
Error	12.42%	10.64%	11.47%	0.51%	12.97%	1.82%	1.52%
(Position)		(0.83, 0.45)[f]	$y = 0.872$	$x = 0.0454$	$y = 0.09$	$y = 1$	

[a] Calculated by integral of velocity function, $\psi = 1.173$.
[b] Calculated by integral of velocity function, $\psi = 5.084$.
[c] Calculated by integral of velocity function, $\psi = 9.107$.
[d] In a symmetric position 0.30, 0.60 there a similar value, ($\psi = 9.225$).
[e] Calculated by integral of velocity function, $\psi = 15.7$.
[f] In a symmetric position 0.17, 0.55 there a similar value ($\psi = 14.656$).

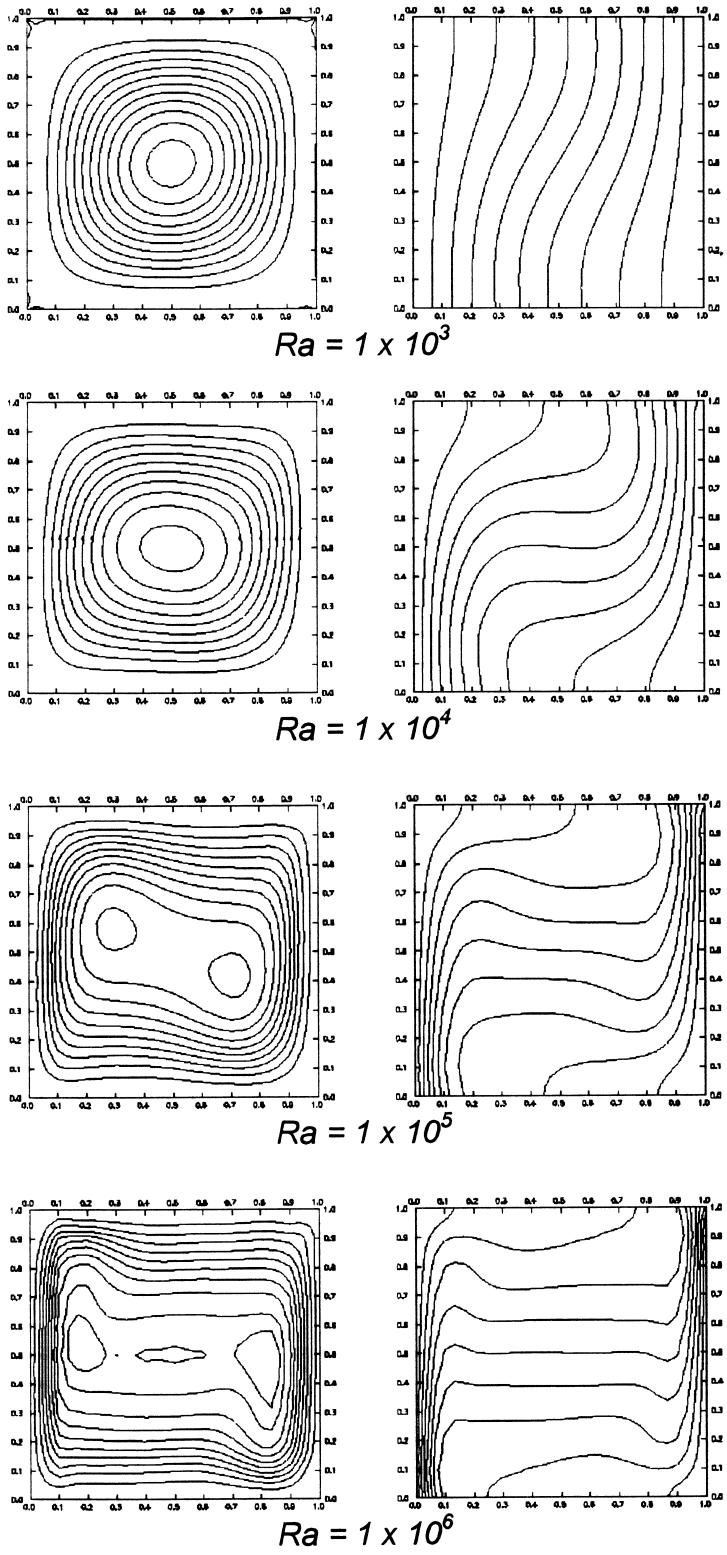

Fig. 2. Numerical predictions of flow patterns and constant temperature lines.

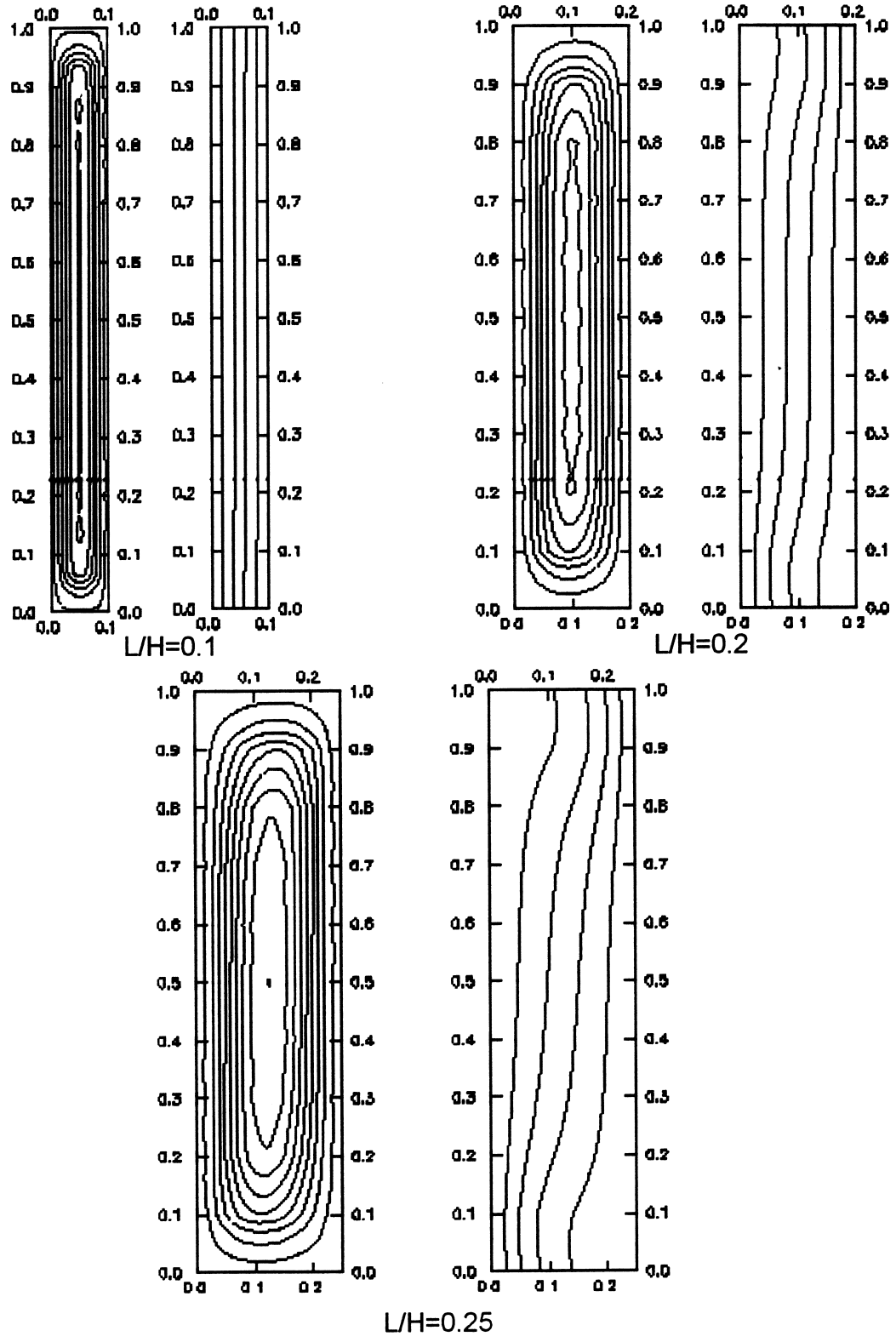

Fig. 3. Stream function patterns and isotemperature curves for various L/H ratios.

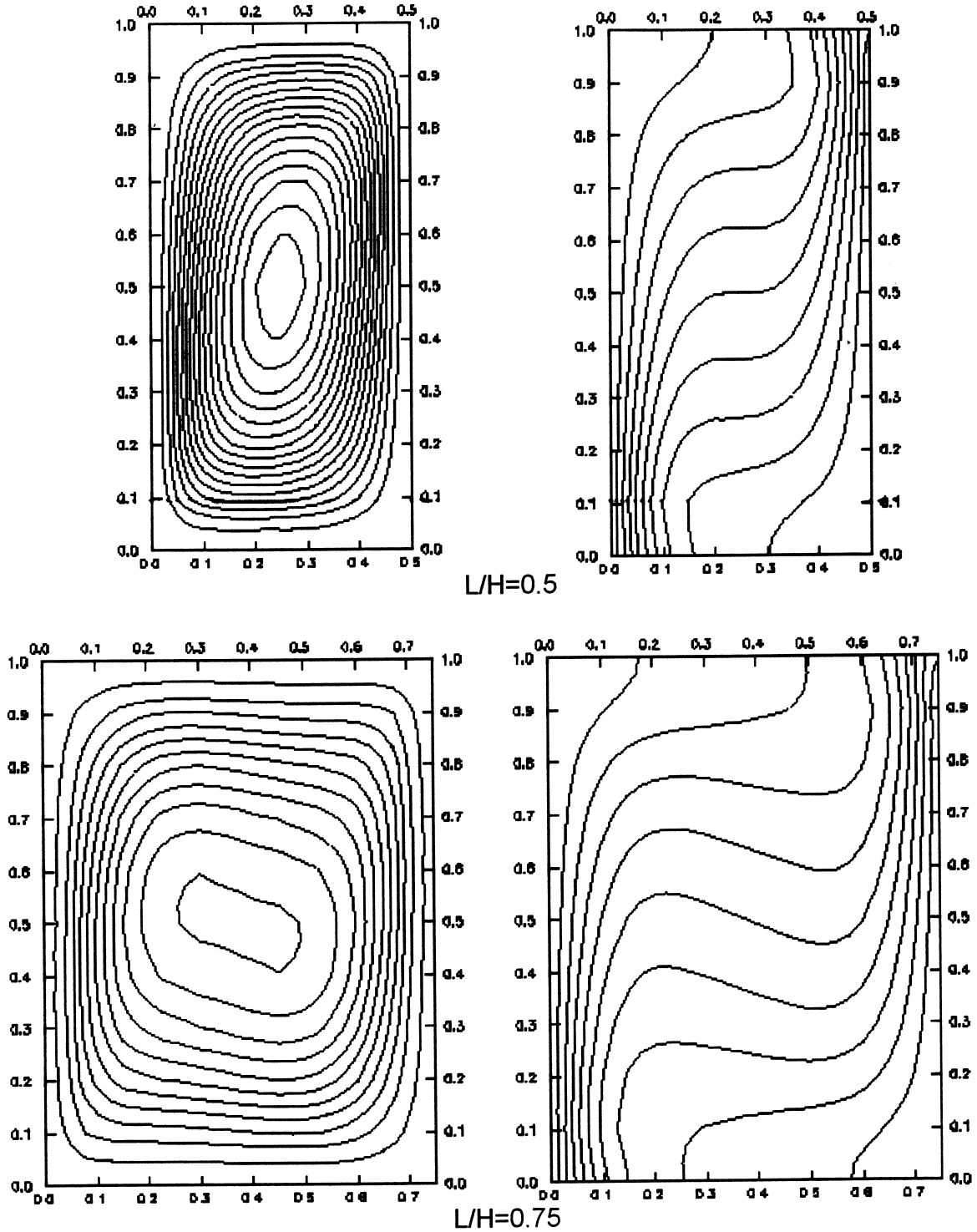

Fig. 4. Stream function patterns and isotemperature curves for various ratios of L/H.

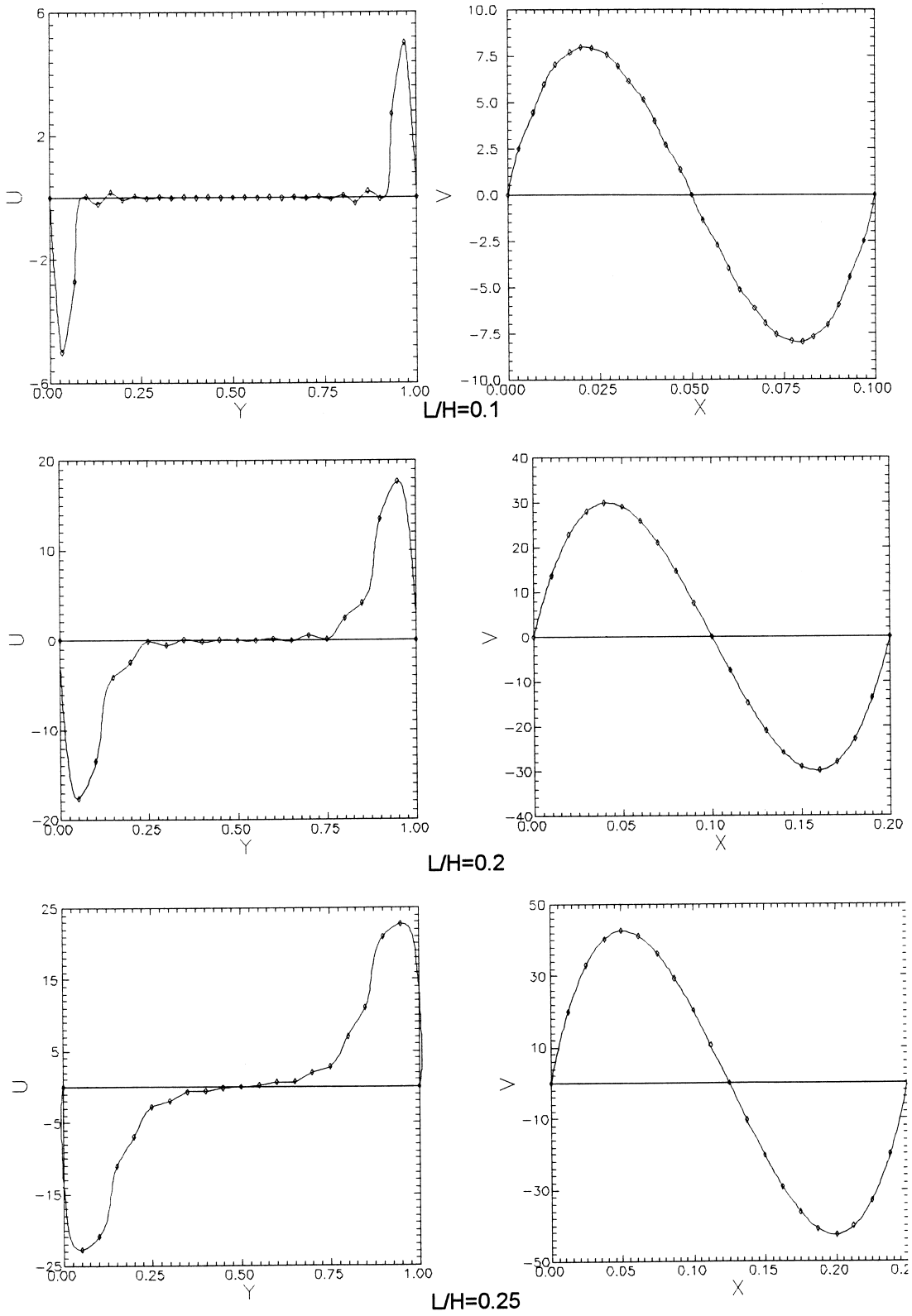

Fig. 5. Velocity profiles for several L/H values.

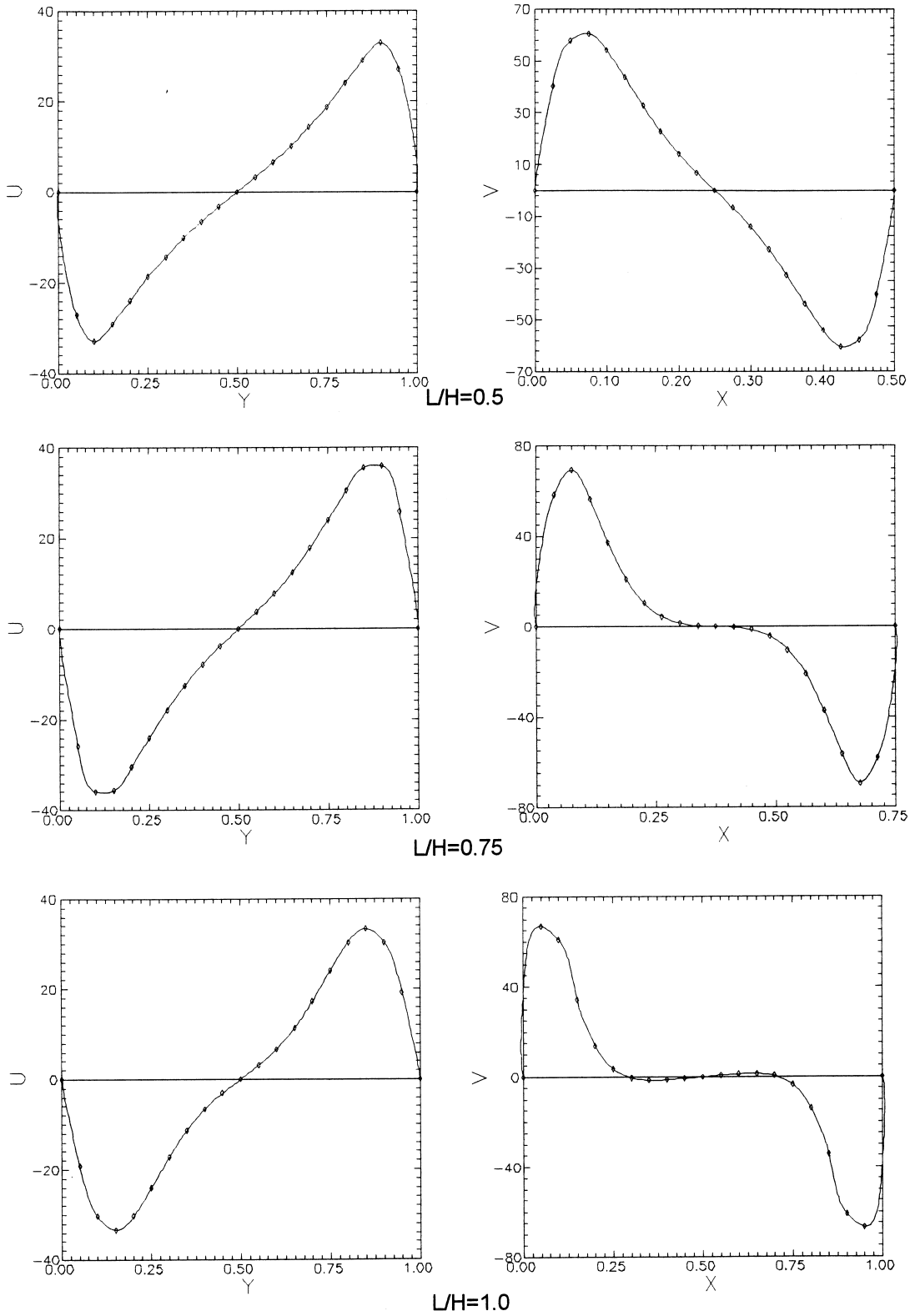

Fig. 6. Velocity profiles for several L/H ratios.

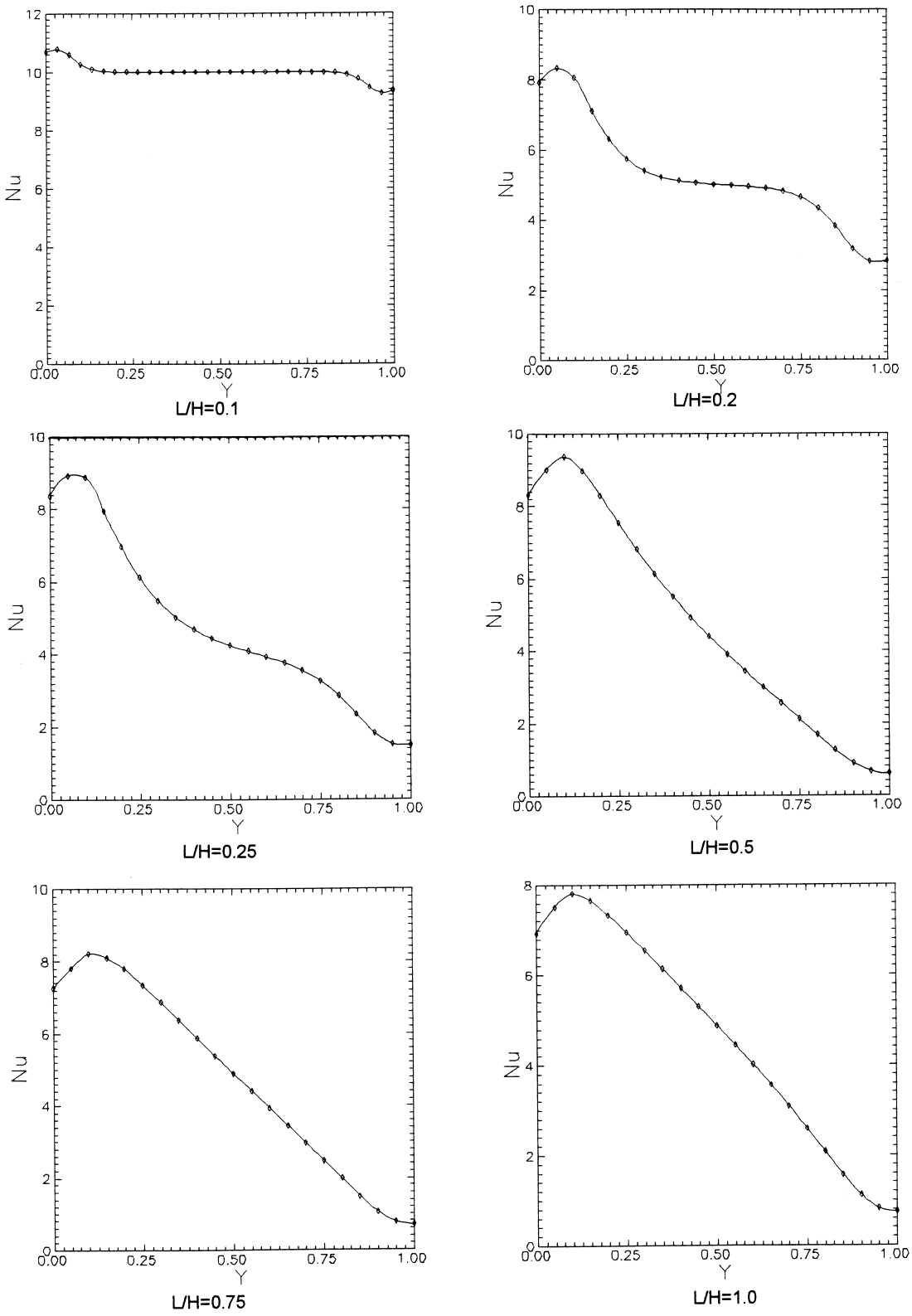

Fig. 7. Nusselt numbers for several L/H ratios.

metries of the cavity and for Rayleigh number $= 10^5$. In the case of $L/H = 0.1$, the stream lines are almost straight over the whole length of the cavity and the temperature profiles are nearly constant indicating that the process of heat transfer across the cavity is basically dominated by conduction. The increase of the cavity width or increasing the ratio L/H to 0.2 and 0.25, one can observe the rapid changes occurring in the stream lines and the temperature profiles indicating an increase of the convection participation in the heat transfer process. In Fig. 4, the ratio of L/H is of 0.5 and 0.75, one can observe the variation of the stream lines patterns and the temperature profiles indicating that convection process is progressively dominating the process of heat transfer. When $L/H = 1$ as in Fig. 2 the heat transfer process is basically controlled by convection as indicated by the corresponding stream lines and the temperature profiles.

Figure 5 shows the variations in the velocity profiles U and V along the vertical and horizontal lines passing by the geometrical center of the cavity for $L/H = 0.1$; 0.2 and 0.25. One can observe that when $L/H = 0.1$, the variation of the velocity U along the vertical line passing by the cavity center is more concentrated at the top and bottom extremities of the cavity while along the remaining part of the cavity length there is no variation. As the ratio L/H increases to the values of 0.2 and 0.25, the regions of variation of the velocity U are extended away from the top and bottom extremities until eventually U varies along the whole length of the cavity as nearly the case when $L/H =$ 0.25. Figure 6 shows the cases of $L/H = 0.50$; 0.75 and 1.0 where the velocity profile U changes and is completely asymmetrical. These variations are expected based upon the stream lines patterns for these cases. The variation of the velocity V along a horizontal line passing by the center of the cavity, for values of $L/H = 0.1$; 0.2 and 0.25; are shown in Fig. 5 and $L/H = 0.5$; 0.75 and 1.0 in Fig. 6. One can notice the variations in the velocity profiles caused by the variation of the ratio L/H.

The variation of the Nusselt number as function of L/H is shown in Fig. 7. One can notice that in case of low L/H, that is, $L/H = 0.1$ the variation of the Nusselt number is limited to the top and bottom extremities of the cavity. When the ratio L/H is increased the Nusselt number greatly changes along the cavity length indicating a maximum value at about 0.1 from the top. Away from the extremity one can observe a nearly linear reduction of the value of Nusselt number along the cavity length as is demonstrated in Fig. 7 for the cases $L/H = 0.75$ and 1.0.

Figure 8 shows the variation of the value of the maximum velocity U_{max} in terms of the ratio L/H. As can be seen the value of U_{max} increases with the increase of the ratio L/H. The eventual reduction in

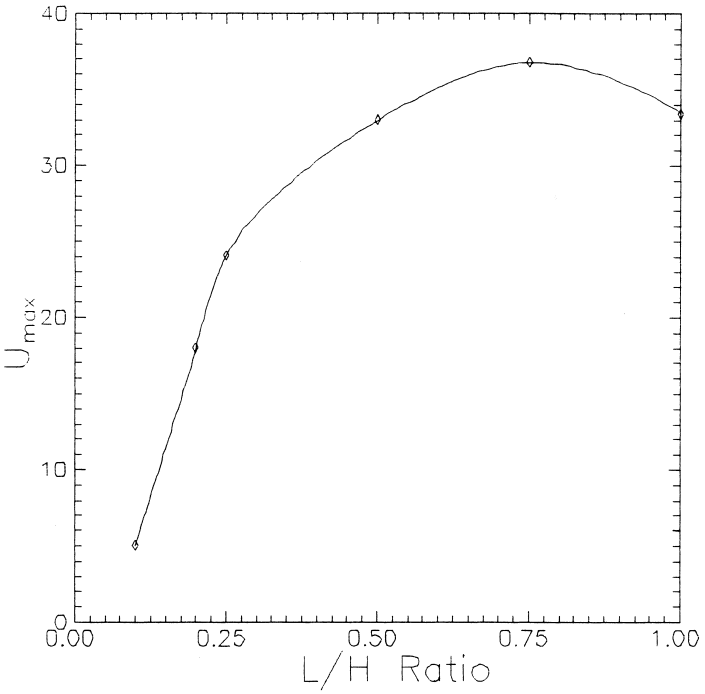

Fig. 8. Variation of U_{max} with ratio L/H.

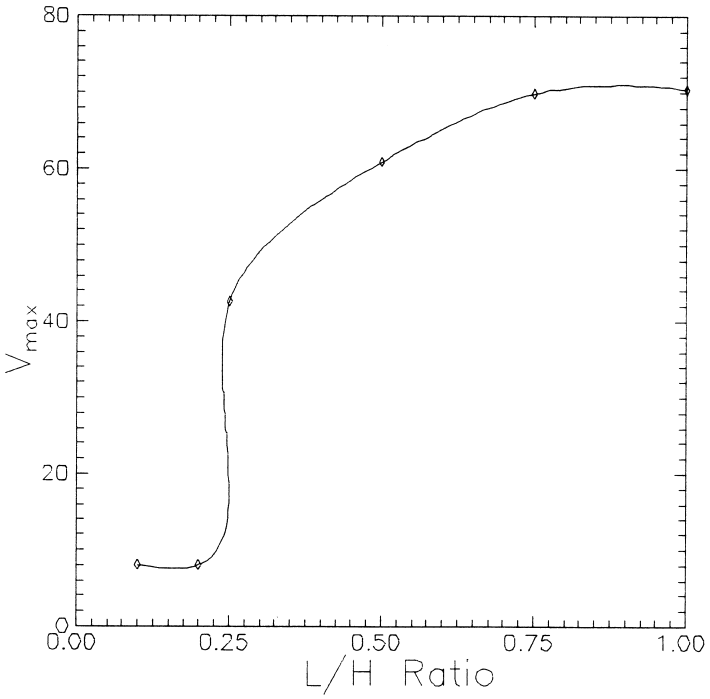

Fig. 9. Variation of V_{max} with ratio L/H.

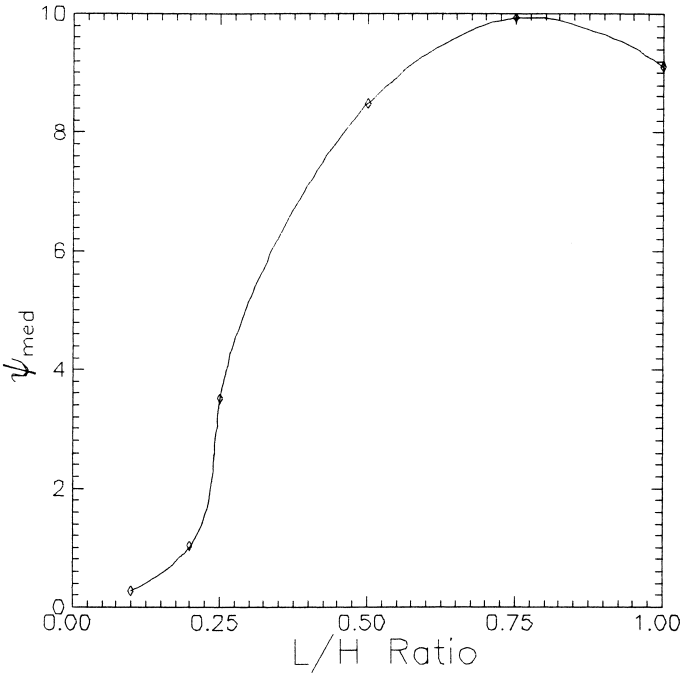

Fig. 10. Variation of the ψ_{med} with the ratio L/H.

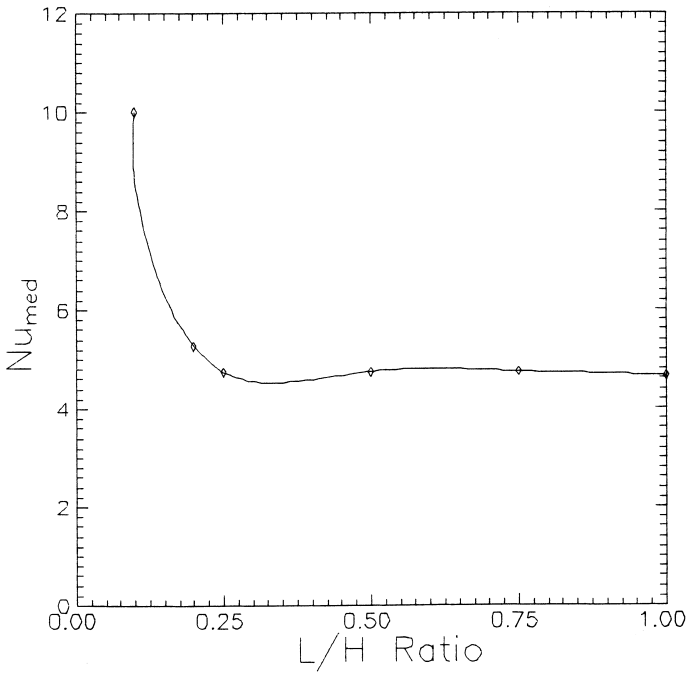

Fig. 11. Variation of mean Nusselt number with the ratio L/H.

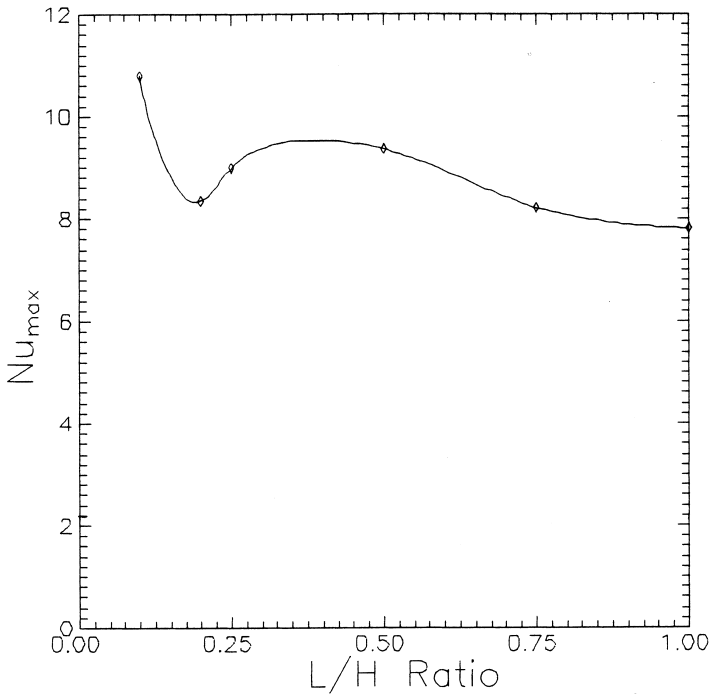

Fig. 12. Variation of the maximum value of Nusselt number with the ratio L/H.

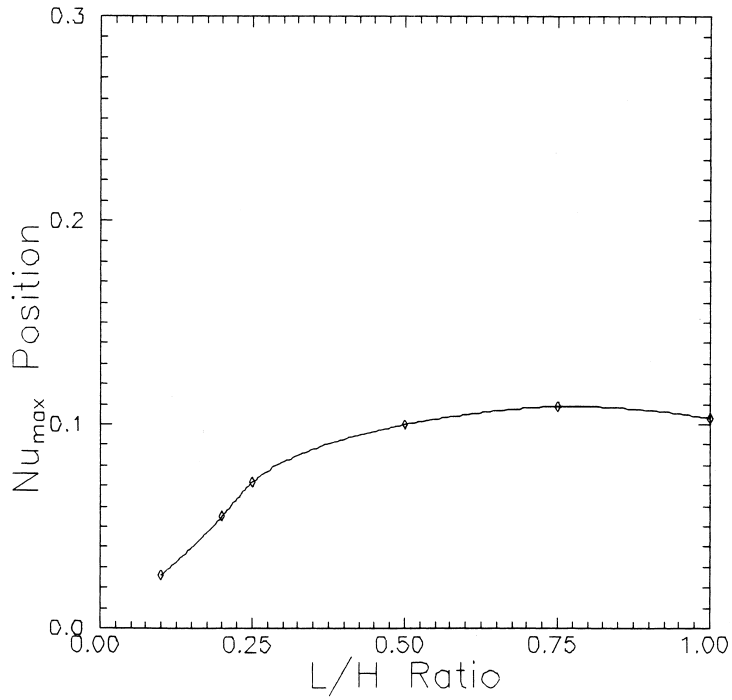

Fig. 13. Variation of the position of Nu_{max} in terms of the ratio L/H.

the case of $L/H = 1.0$ is basically due to the commencement of vortices in the central part of the cavity where the point of maximum velocity is moved away from the central line. The variation of the maximum velocity V_{max} is shown in Fig. 9 and indicates similar behavior to that of U_{max}.

Figure 10 shows the variation of the maximum value of the stream function ψ_{max} in terms of the ratio L/H. As can be seen, the maximum value of ψ, that is ψ_{max} increases with the increase of the ratio L/H, until for $L/H = 1.0$, the recirculation starts in the central region in the form of two recirculating vorticities.

The variation of the mean Nusselt number in terms of the ratio L/H is shown in Fig. 11. One can observe that, for values of L/H below 0.25, the mean Nusselt number is reduced when the ratio L/H is increased due to the fact that heat conduction dominates the heat transfer process in this range of L/H. For larger values of L/H, that is, $L/H \geq 0.5$, the mean Nusselt number seems to be unaffected by the variation of the ratio L/H. In this range of L/H the heat transfer process is strongly dominated by the free convection mechanisms of heat transfer as pointed out when discussing the stream function patterns and the associated temperature profiles. In the region of $0.25 \leq L/H \leq 0.5$, both decaying weak conduction and increasingly dominant free convection effects are simultaneously present leading to slight increase in the heat transfer rate until it reaches a stable value at around $L/H \approx 0.5$, where only free convection dominates the heat transfer process.

The variation of the maximum value of the Nusselt number with the variation of the ratio L/H is presented in Fig. 12 where the maximum value is continuously decreasing due to the increase of the ratio L/H and the corresponding decrease of the temperature gradient across the gap. As the gap width increases, that is, the ratio L/H increases, the heat transfer by conduction is further reduced while the free convection effects starts to be stronger resulting in recuperating the heat transfer rate and increasing the local maximum value of the Nusselt number. Further increase of the gap ratio leads to stronger free convection effects dominating the heat transfer process and stabilizing both the heat transfer rate and the corresponding Nusselt number. Fig. 13 shows how the location of occurrence of the maximum value of Nusselt number moves as a result of the variation of the ratio L/H and remains nearly in a fixed region at high values of L/H, where free convection is well established and dominant.

4. Conclusions

The present study shows that the proposed model and the method of solution predict results that compare well with the bench mark solution and the Vahl

Davis' results. Also the method allows for routine solutions for the cases of high Rayleigh number. Better predictions are possible by using fine grids. Further, the stream function patterns, the temperature and velocity profiles as well as the Nusselt number were investigated in terms of the variation of the Rayleigh number and the ratio L/H of the cavity.

Acknowledgements

The authors wish to thank the Brazilian National Research Council for the scholarship and the financial support to the research project number 521235/97-9

References

[1] R. Marshall, J. Heinrich, O. Zienkiewicz, Natural convection in a square enclosure by a finite-element, penalty function method using primitive fluid variables, Num. Heat Transf. 1 (1978) 331–349.
[2] G. Schneider, G. Raithby, M. Yvanovich, Finite-element solution procedures for solving the incompressible, Navier–Stokes equations using equal order interpolation, Num. Heat Transf. 1 (1978) 433–451.
[3] P. Gresho, On the theory of semi-implicit projection methods for viscous incompressible flow and its implementation via finite element method that also introduces a nearly consistent mass matrix, Int. J. Num. Meth. Fluids 11 (1990) 587–620.
[4] P. Gresho, S.T. Chan, On the theory of semi-implicit projection methods for viscous incompressible flow and its implementation via finite element method that also introduces a nearly consistent mass matrix, Int. J. Num. Meth. Fluids 11 (1990) 621–659.
[5] C. Prakash, An improved control volume finite-element method for heat and mass transfer and for fluid flow using equal-order velocity–pressure interpolation, Num. Heat Transf. 9 (1986) 253–276.
[6] M. Perıc, R. Kessler, Scheurer, Comparison of finite-volume numerical methods with staggered and co-located grid, Comput. Fluids 16 (1988) 389–403.
[7] J. Rice, R. Schnipke, An equal-order velocity pressure formulation that does not exhibit spurious pressure modes, Comp. Meth. Appl. Mechanical Eng. 58 (1986) 135–149.
[8] A Kovacs, M. Kawahara, A finite element scheme based on the velocity correction method for the solution of the time-dependent incompressible Navier–Stokes equations, Int. J. Num. Meth. Fluids 12 (1991) 403–423.
[9] G. Ren, T. Utnes, A finite element solution of the time-dependent incompressible Navier–Stokes equations using a modified velocity correction method, Int. J. Num. Meth. Fluids 17 (1993) 349–364.
[10] G. Despotis, S. Tsangaris, Fractional method for solution of incompressible Navier–Stokes equations on unstructured triangular meshes, Int. J. Num. Meth. Fluids 20 (1995) 1273–1288.
[11] A. Brooks, T. Hughes, Streamline Upwind/Petrov-Galerkin formulations for convection dominated flows with particular emphasis on the incompressible Navier–Stokes equations, Comp. Meth. Appl. Mechanical Eng. 32 (1982) 199–259.
[12] J. Rice, R. Schnipke, A monotone streamline upwind finite elements method for convection-dominated flows, Comp. Meth. Appl. Mechanical Eng. 48 (1985) 313–327.
[13] B. Baliga, S. Patankar, A new finite element formulation for convection–diffusion problems, Num. Heat Transfer 3 (1980) 393–409.
[14] B. Baliga, S. Patankar, A control volume finite element method for two dimensional fluid flow and heat transfer, Num. Heat Transfer 6 (1983) 245–261.
[15] C. Prakash, S. Patankar, A control volume-based finite-element method for solving the Navier–Stokes equations using equal-order velocity–pressure interpolation, Num. Heat Transfer 8 (1985) 259–280.
[16] H. Saabas, B. Baliga, Co-located equal order control-volume finite element method for multidimensional incompressible flow — Part I: formulation, Num. Heat Transfer 26 (1994) 381–407.
[17] S. Idelsohn, E. Oñate, Finite volumes and finite elements: two 'good friends', Int. J. Num. Meth. Eng. 37 (1994) 3323–3341.
[18] G. Vahl Davis, I. Jones, Natural convection in a square cavity: a comparison exercise, Int. J. Num. Meth. Fluids 3 (1993) 227–248.
[19] G. Vahl Davis, Natural convection of air in a square cavity: a bench mark numerical solution, Int. J. Num. Meth. Fluids 3 (1983) 249–264.